IEEE Author Portal IEEE Access

Special Section: Planar Microwave Sensors

A compact Vivaldi-shaped array using antipodal Vivaldi antennas to stabilize the high-frequency radiation pattern

Submission ID 04a9faa9-38a5-4e4a-97ca-2cc415aabff1

Submission Version Initial Submission

PDF Generation 25 Nov 2024 12:12:13 EST by Atypon ReX

Authors

Mr. JULIEN HAREL
Corresponding Author
Submitting Author

Affiliations
- CNRS, IETR (Institut d'Électronique et des Technologies du numéRique)—UMR 6164, Univ Rennes, Rennes, France
- Avantix SAS, Aix-En-Provence, France

Prof. MOHAMED HIMDI

Affiliations
- CNRS, IETR (Institut d'Électronique et des Technologies du numéRique)—UMR 6164, Univ Rennes, Rennes, France

Prof. OLIVIER LAFOND

Affiliations
- CNRS, IETR (Institut d'Électronique et des Technologies du numéRique)—UMR 6164, Univ Rennes, Rennes, France

Dr. OLIVIER CLAUZIER

Affiliations
- Avantix SAS, Aix-En-Provence, France

Mr. OLIVIER VIVARES

Affiliations
- Avantix SAS, Aix-En-Provence, France

Additional Information

Keywords

5G mobile communication

Arrays

Beam steering

Ultra wideband antennas

Vivaldi antennas

Subject Category

Antennas and propagation

Electromagnetic compatibility and interference

Files for peer review

All files submitted by the author for peer review are listed below. Files that could not be converted to PDF are indicated; reviewers are able to access them online.

Name	Type of File	Size	Page
Article_IEEE_Access_final draft.pdf	Main Document - PDF	8.7 MB	Page 3

IEEE Access
Multidisciplinary ⋮ Rapid Review ⋮ Open Access Journal

Date of publication xxxx 00, 0000, date of current version xxxx 00, 0000.

Digital Object Identifier 10.1109/ACCESS.2023.1120000

A compact Vivaldi-shaped array using antipodal Vivaldi antennas to stabilize the high-frequency radiation pattern

JULIEN HAREL[1], MOHAMED HIMDI[1], OLIVIER LAFOND[1], OLIVIER CLAUZIER[2], and OLIVIER VIVARES[2]
[1]CNRS, IETR (Institut d'Électronique et des Technologies du numéRique)—UMR 6164, Univ Rennes, Rennes, France
[2]Avantix SAS, Aix-En-Provence, France

Corresponding author: Julien HAREL (e-mail: julien.harel@univ-rennes.fr).

This work is supported by AVANTIX SAS, the European Union through the European Regional Development Fund (ERDF), and by the Ministry of Higher Education and Research, Brittany, Rennes Métropole and Conseils Départementaux 35 and 22, through the CPER Projects SOPHIE / STIC & Ondes and CyMoCoD.

ABSTRACT In this study, a novel ultra-wideband antipodal Vivaldi antenna with a Chebyshev tapering profile and exponential slots is designed and measured. The dimensions of the proposed antenna are 95mm x 100mm x 0.127mm and the relative dimensions are $0.285\lambda_0$ x $0.3\lambda_0$ x $0.0004\lambda_0$ where λ_0 is the free space wavelength at the lowest operating frequency at 0.9 GHz. Several array configurations are proposed and all elementary array sources are combined in a mirror configuration, including the feeding part, to drastically reduce cross-polarization. First, a planar array is created at a distance $d = 150mm$ between elementary sources. Then, from this primary source, an oblique array is created by inclining the two antennas at an angle θ, which cancels the ambiguity lobes in the upper frequency band. Finally, the single antenna is bent along a Vivaldi curvature, creating a mechanical tilt depending on the curvature parameters in H-plane. An array is formed by two curved Vivaldi antennas and exhibits a tilting effect with better compactness than the oblique array. For measurements, several foams with Vivaldi curvatures were created, allowing us to shape the Vivaldi antennas along various array distances, resulting in various beam shapes depending on the configuration used. The optimal distance $d = 50mm$ provides a more stable radiation pattern across frequencies and cancels out ambiguity lobes for distances $> 2\lambda_0$. These Vivaldi-shaped arrays are measured and show good agreement with simulations.

INDEX TERMS array, beam shaping, miniaturization, ultra-wideband (UWB), Vivaldi antenna.

I. INTRODUCTION

IN recent needs in wireless communication applications, a common problematic is the need to shape the antenna's radiation pattern in order to meet the application specific demand. Among these applications, we can cite MIMO technologies such as 5G, LTE & WLAN networks, as well as ultra-wideband (UWB) communications, radar and medical imaging. Depending on the application, the required radiation pattern can be either directive, wide, or have dual or multiple beams to improve communication link between transmit antenna and single or various receive antennas, [1]–[3]. Implementing and changing the radiation pattern depending on the application or frequency of an antenna is complex and often requires different types of antennas in the same system to operate, thereby increasing the cost, dimensions and complexity of such system. In this study, we propose a novel UWB antipodal Vivaldi antenna with a Chebyshev tapering and exponential slots to improve its compactness. Then, a dual Vivaldi antenna array arrangement is designed along a Vivaldi shape, allowing to display pattern diversity depending on the chosen spacing between elements in the array. The paper is organized as follows: Section II describes the antenna design and simulation, Section III discusses the array conception with planar, oblique and Vivaldi shaped arrays, Section IV shows the measurements results and Section V provides the conclusion of this research work.

II. ANTENNA DESIGN

The proposed UWB antenna design is based along the Vivaldi antenna, first conceptualized by Gibson in 1979 [4] with microstrip line to slot coupling feed transition, and then improved by Gazit [5] with the antipodal Vivaldi antenna (AVA), which extends the impedance bandwidth through a wideband transition from microstrip line to tapered slot flare.

In order to improve the return loss parameter, a Chebyshev tapering profile, inspired by [6], is added to the topology as shown in Fig. 1 and is designed as follow:

The antenna is fed by an UWB microstrip balun with an elliptical shape and is printed via a silver coating on a PET substrate of relative permittivity 2.7, loss tangent of 0.002 and thickness 0.127mm. In order to achieve a smooth transition between the feed line and the exponential tapered slot, a straight slot line from (x=-W_f ; y=0) to (x=0 ; y=y_1) is created, where W_f is the width of the microstrip feed line. After this, an exponential tapered curve is defined by eq. 1 :

$$x = C_1 e^{Rz} + C_2 \quad (1)$$

while

$$C_1 = \frac{x_2 - x_1}{e^{Rz_2} - e^{Rz_1}} \quad (2)$$

$$C_2 = \frac{x_1 e^{Rz_2} - x_2 e^{Rz_1}}{e^{Rz_2} - e^{Rz_1}} \quad (3)$$

where R is the opening rate of the exponential transition, $P_1(x_1,z_1)$ and $P_2(x_2,z_2)$ are respectively the coordinate positions of the start and end points of the exponentially tapered slot, as indicated by the red dots in Fig. 1. The exponential opening rate R is one of the key parameters to optimize on the Vivaldi antenna in order to influence the VSWR in the low-frequency region [7].

Following [6], a Chebyshev tapering profile, represented by the blue curves in Fig. 1, is defined by eq. (4) to widen the bandwidth with a better impedance matching at low frequencies. The length of this curve is normalized with the variable L_c, then rotated by an angle $\theta = -27.65°$.

$$x = N(\frac{z}{L_c})^4 - N(\frac{z}{L_c})^2 \quad (4)$$

With N the opening rate of the Chebyshev function, and $0 \leq z \leq L_c$.

$$L_c = \sqrt{(\frac{W}{2} - W_f)^2 + z_2^2} \quad (5)$$

Finally, to improve the return loss in the low frequency band, exponential slots (ES) are added to the edges of the antenna in Fig. 2, [8]. These slots allow the surface current to pass through a longer distance around the antenna, hence enhancing the return loss at lower frequencies, as shown in Fig. 3a. These slots are also following a Vivaldi curve, eq. (6), (7) :

$$x = C_3 e^{R_2 z} + C_4 \quad (6)$$

$$x = C_5 e^{R_3 z} + C_6 \quad (7)$$

with

$$C_3 = \frac{x_4 - x_3}{e^{R_2 z_4} - e^{R_2 z_3}} \quad (8)$$

TABLE 1. Geometrical dimensions of the proposed antenna

Parameters	Value (mm)
W_f	0.325
L	95
W	100
x_1	0
z_1	50
x_2	41.8375
z_2	84
x_3	5
z_3	30
x_4	49.8375
z_4	60.35
x_5	9
z_5	30
x_6	49.8375
z_6	60
R_x	48.4
R_z	15

$$C_4 = \frac{x_3 e^{Rz_4} - x_4 e^{R_2 z_3}}{e^{R_2 z_4} - e^{R_2 z_3}} \quad (9)$$

$$C_5 = \frac{x_6 - x_5}{e^{R_3 z_6} - e^{R_3 z_5}} \quad (10)$$

$$C_6 = \frac{x_5 e^{R_3 z_6} - x_6 e^{R_3 z_5}}{e^{R_3 z_6} - e^{R_3 z_5}} \quad (11)$$

The optimal parameters of geometrical dimensions of the Chebyshev AVA given by parametric studies to improve the impedance bandwidth are listed in Table 1. The optimal parameters for R is 0.16, R_2 is 0.2, R_3 is 0.09 and N is 70.

The simulated return loss of these antennas are depicted on Fig. 4. The AVA Chebyshev antenna shows a good $VSWR <$ 2.2 starting from 1.1 GHz and up to 35 GHz, whereas the AVA Chebyshev with exponential slots shows a $VSWR < 2.8$ starting from 0.9 GHz and up to 35 GHz. By comparing both antennas at the same VSWR, $VSWR < 2.8$ is achieved at 1 GHz for the AVA Chebyshev and 0.9 GHz for the AVA Chebyshev ES, showing a dimension improvement by reducing the length and width by 10%. We can note that $VSWR < 1.9$ is achieved for the AVA Chebyshev at 1.12 GHz, whereas the Chebyshev ES can achieve the same VSWR at 0.98 GHz. However, a rise of return loss is observed with a maximum at 3 GHz in both cases, with a $VSWR = 2.2$ for the AVA Chebyshev case, and $VSWR = 2.8$ for the Chebyshev ES case. The relative dimensions of the AVA Chebyshev ES towards λ_0 are $0.285\lambda_0$ x $0.3\lambda_0$ (L x W), where λ_0 is the free space wavelength at the lowest operating frequency, here 0.9 GHz.

III. ARRAY CONCEPTION

A. PLANAR AND OBLIQUE ARRAY

In order to improve the directivity of the antenna, an array in the H-plane is created by adding a second Vivaldi antenna

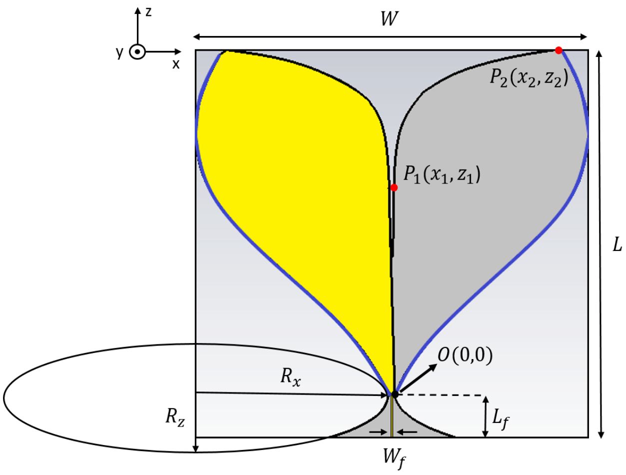

FIGURE 1. Geometry of the Chebyshev AVA

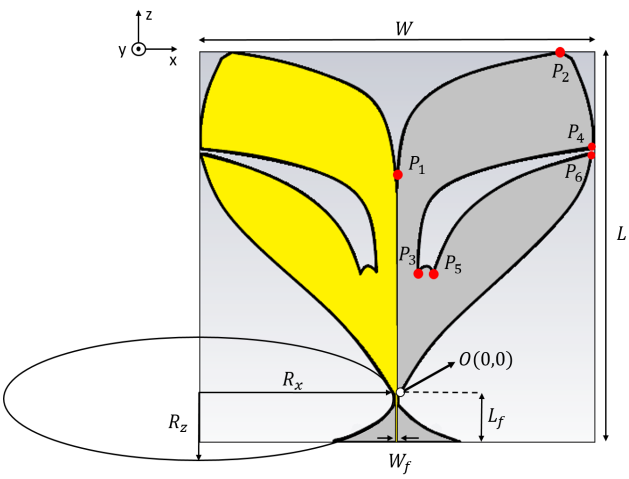

FIGURE 2. Geometry of the Chebyshev AVA with exponential slots

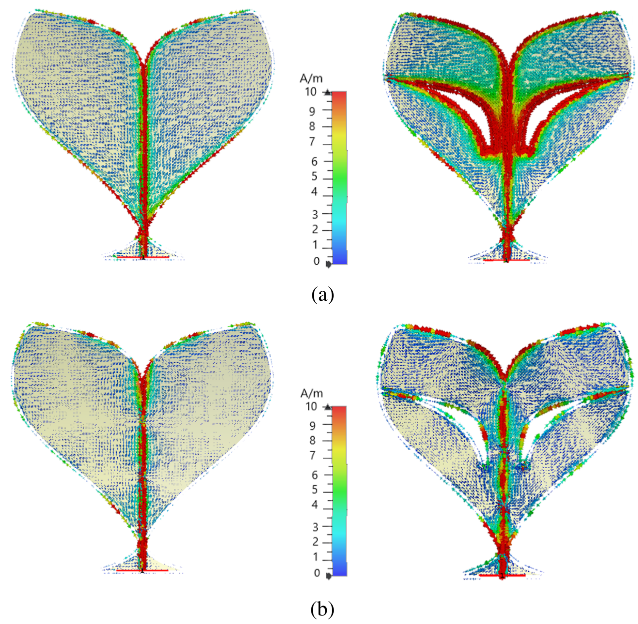

FIGURE 3. Comparison of surface current distribution of the AVA Chebyshev and AVA Chebyshev ES at frequencies (a) 1 GHz; (b) 6 GHz

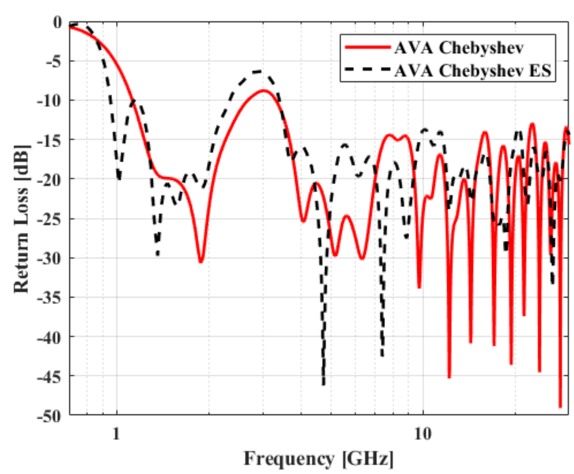

FIGURE 4. Simulated return loss of the AVA Chebyshev with (black dots) and without (red line) exponential slots

at a distance $d = \frac{\lambda_{1GHz}}{2}$ at 1 GHz (i.e. $d = 150mm$), (Fig. 5a). The second antenna is a mirrored version of the first one along the x axis, allowing the orthogonal components of the E-field (corresponding to the cross polarization) to cancel each other at broadside [9], (Fig. 5b). In this particular case, it is crucial that the Co-polarization of the E-field of both antennas are emitted in the same direction, which requires that the "top face" of each antenna are facing each other. This configuration permits to lower the Cross-polarization level at broadside by an average of 30dB over the entire bandwidth, while the Co-polarization stay at the same level in both case, Fig. 6.

However, the array factor of the combined radiation pattern contributes to significant grating lobes at higher frequencies because the distance becomes $2\lambda_0$ at 3 GHz and $3\lambda_0$ at 6 GHz. To mitigate the grating lobe level at high frequencies, it is possible to orient the elements at an oblique angle α [10], as determined by eq. 12. An illustration of such an oblique array, with a maximum distance of $d = 150mm$ corresponding to an angle of $\alpha = 52.1°$, is presented in Fig. 7.

$$\alpha = sin^{-1}\frac{d/2}{L} \quad (12)$$

The mitigation of grating lobes is obtained via the tapered slot of the Vivaldi antenna : in theory, electromagnetic waves at lower frequencies are emitted primarily through the end of the exponential aperture, while those at higher frequencies predominantly radiate from the slot's beginning (see Fig. 8b). Introducing an oblique angle results in varying distances within the array for low and high frequencies, allowing to improve the directivity at low frequencies while reducing the grating lobe level at high frequencies. By progressively increasing this angle, the separation between the two antennas linearly expands, enhancing the directivity across both low and high frequencies [10].

The oblique configuration of the array also induces a tilt in the radiation pattern within the H-plane, tilt of the same value as the angle α. At high values of angle, this tilt will decreases the array's directivity because the radiation patterns of both antennas are not pointing in the same direction, hence

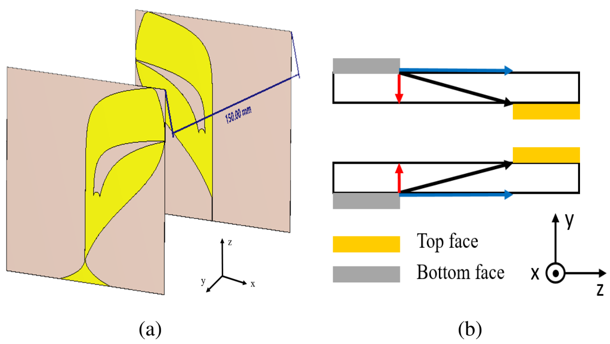

FIGURE 5. **(a) H-plane planar array with mirrored AVA at d=150mm; (b) E-field direction of the mirrored AVA array**

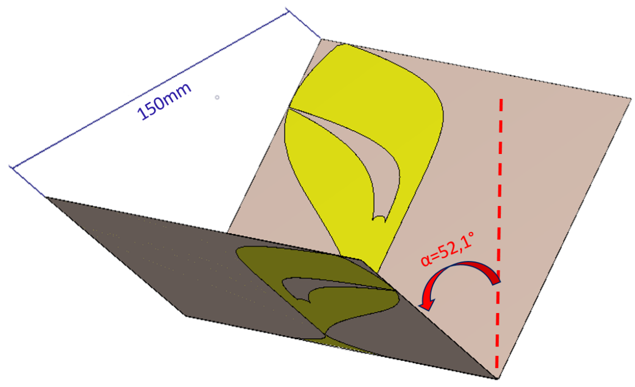

FIGURE 7. **H-plane oblique array with mirrored AVA at d=150mm**

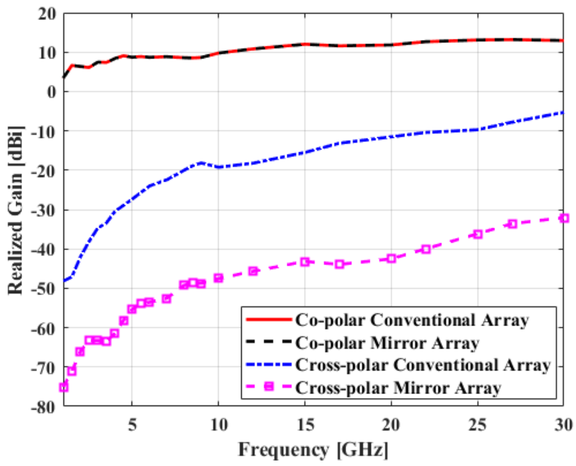

FIGURE 6. **Comparison between Co & Cross polarization level of the conventional & mirrored planar array with d = 150mm at broadside**

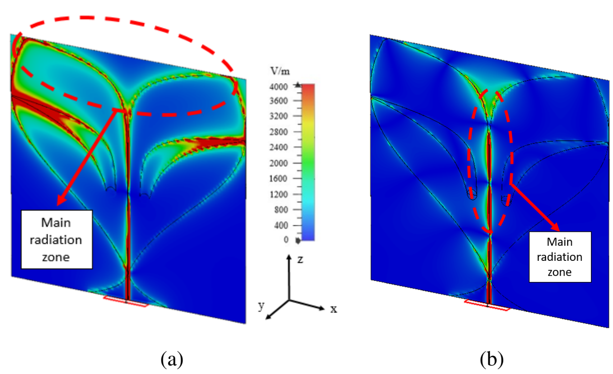

FIGURE 8. **E-field distribution of the AVA Chebyshev ES at frequencies of (a) 1 GHz; (b) 6 GHz**

reducing the array factor. Since the radiation pattern in H-plane is quasi-omnidirectional due to the dipole-type nature of Vivaldi antenna at low frequencies, there will always be an array factor as shown in Fig. 9a at 1 GHz. However, the reduction in directivity becomes effective when the radiation pattern of the individual antenna becomes directive and tilted at higher frequencies (e.g. 6 GHz, Fig. 9b).

B. CURVED ARRAY IN VIVALDI SHAPE

In order to improve the mechanical beam tilt and the compactness of the oblique array, an array formed by two Vivaldi antennas bent along a Vivaldi curvature, eq. (1), was designed. As this array aims to optimize the effect of the array spacing along the antenna on the radiation pattern, several Vivaldi curvatures were created to realize different distances d : 50mm ; 100mm and 150mm. All Vivaldi curvatures have the same opening rate $R = 0.06$.

1) Single antenna curved

In the first place, the AVA Chebyshev ES is bent alone along various Vivaldi curvatures to observe the different effects taking place, Fig. 10. The different cases $d = 50mm$, $d = 100mm$ and $d = 150mm$ referred to in this section correspond to the same distances used in the array case. First, the return loss is the same as the planar antenna. This can be explained by the nature of the Vivaldi antenna which is a travelling wave antenna. While bending the antenna, surface current can still follow the antenna profile, thus creating a radiating field in the exponential tapering area. In the same way as the oblique case, the radiating field will also follow the applied bending, hence creating a tilting effect which can be seen on the radiation pattern in H-plane.

By comparing the Vivaldi and oblique curvatures on an antenna alone, we observe an enhancement of the tilt angle with the Vivaldi configuration, which can be seen in the $d = 100mm$ & $d = 150mm$ cases at 6 GHz in Fig. 11. For the $d = 150mm$ case, the oblique configuration exhibits a tilt angle of $52.1°$, whereas the Vivaldi configuration achieves a tilt angle of $69.9°$, therefore increasing the beam tilt angle by approximately $18°$ while maintaining the same compactness. Table 2 shows a comparison of tilt angles between the Vivaldi and oblique arrangements, depending on the maximum distances between radiators. We can see that the Vivaldi curve always demonstrates a greater tilting effect, and that there is an $\approx$ 2 factor on distance to achieve the same tilt angle between the $d = 50mm$ Vivaldi case and the $d = 100mm$ oblique case.

Although it is easy to estimate the tilt angle produced by the oblique antenna, which will theoretically be the same as the applied oblique angle, it is difficult to predict the tilt angle produced by the curved case. Indeed, one could say that the tilting angle would be correlated to the end point of the

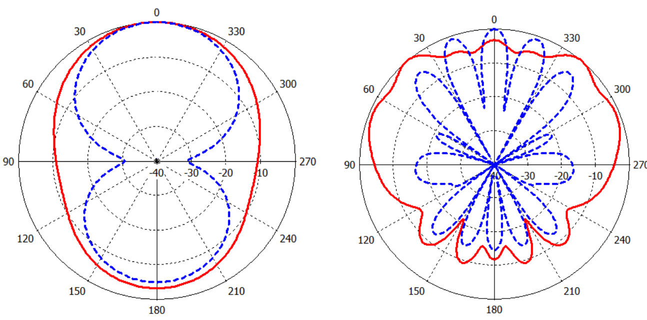

(a) (b)

FIGURE 9. Normalized simulated H-plane Co-polar (blue dots) of the AVA planar array d=150mm & Co-polar (red line) of the oblique array d=150mm at (a) 1 GHz; (b) 6 GHz

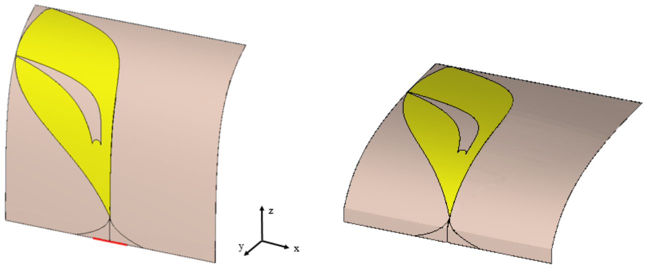

(a) (b)

FIGURE 10. H-plane Vivaldi curved alone at (a) d=50mm; (b) d=150mm

antenna. By calculating the tangent line, eq. (13) to that point, i.e. $y_0 = y_{max-th}$, and then calculate the angle by eq. (14), we found no correlation between the theoretical θ_{max-th} and the average tilt angle value θ_{sim} retrieved from simulation as shown in table 3. However, by calculating the theoretical tilt angle at a closer point of the antenna's curvature y_{av-th}, we found a good correlation between theoretical and simulated tilt angle value, showing that with a specific curvature like the Vivaldi's, the antenna does not radiate from its end point but at a closer point, as illustrated in Fig. 12. By doing a percentage of z_{av-th} to z_{max-th} for each Vivaldi curvatures, we can see that the theoretical radiating point is located approximately at 80.2% of z_{max-th} in z axis. It is important to note that this tilt angle is varying along frequency, but becomes stable at higher frequency.

$$z = f'(y_0) * (y - y_0) + f(y_0) \tag{13}$$

TABLE 2. Comparison of tilt angle for the oblique and Vivaldi curvature various distances

Distance (mm)	Arrangement	Tilt angle (°)
50	Oblique	15,2
	Vivaldi	30,4
100	Oblique	31,7
	Vivaldi	51,3
150	Oblique	52,1
	Vivaldi	69,9

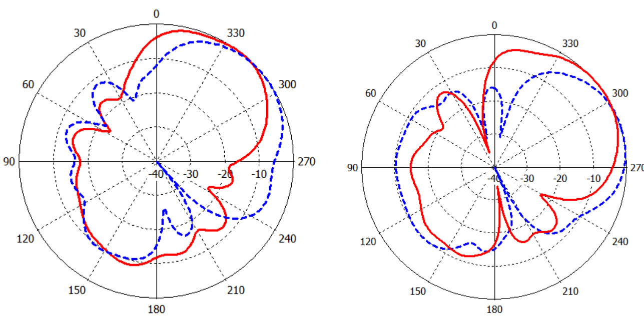

(a) (b)

FIGURE 11. Normalized H-plane radiation pattern of the antenna alone with an oblique (red line) and Vivaldi (blue dots) arrangements at 6 GHz (a) d=100m; (b) d=150mm

TABLE 3. Comparison of theoretical and simulated tilt angles and associated *z* values for the Vivaldi curvature at various distances

Distance (mm)	θ_{max-th} (°)	z_{max-th} (mm)	θ_{sim} (°)	z_{av-th} (mm)
50	56,5	87,22	30,4	71,6
100	71,9	70,5	51,3	55,7
150	78,5	47,3	69,9	37,5

$$\theta_{theo} = tan^{-1}\frac{y_0 + b_{tg}}{z_0} \tag{14}$$

with

$$b_{tg} = z_0 - f'(y_0) * y_0 \tag{15}$$

$$f(y_0) = C_{1viv} * e^{Rz} + C_{2viv} \tag{16}$$

$$f'(y_0) = C_{1viv} * Rz * e^{Rz} \tag{17}$$

2) Curved array

In the same way as the planar and oblique arrays, a mirrored version of the curved antenna is made to create the Vivaldi curved arrays arrangement. Three curved arrays with distances at the end point of the antenna d : 50mm (Fig. 13a); 100mm and 150mm (Fig. 13b) are designed and simulated. These distances are chosen to maximize the array factor at low frequencies for high values of d ($d = 150mm$ corresponding to $\frac{\lambda}{2}$ at 1 GHz) or for higher frequencies ($d = 50mm$ corresponding to $\frac{\lambda}{2}$ at 3 GHz). The excitation of this array is carried out as follows : we aim to minimize the distance between antennas in order to optimize the array factor in the high-frequency radiation zone, thus, we selected a stripline feed for the array. To achieve this, we positioned two antennas so that their 'top face' copper lines touch at the base, forming an array with an excitation similar to a balanced antipodal Vivaldi antenna [11], Fig. 14. As the excitation type transitions from microstrip to stripline, it is necessary to adjust the width of the feed line to achieve a 50Ω impedance matching, by reducing the width from $wf = 0.325mm$ to $wf = 0.14mm$. To ensure accurate software simulation, the excitation is planar over 6mm before bending the antennas.

The directivity of the oblique array at $d = 150mm$ is compared to the Vivaldi curved array at various distances in

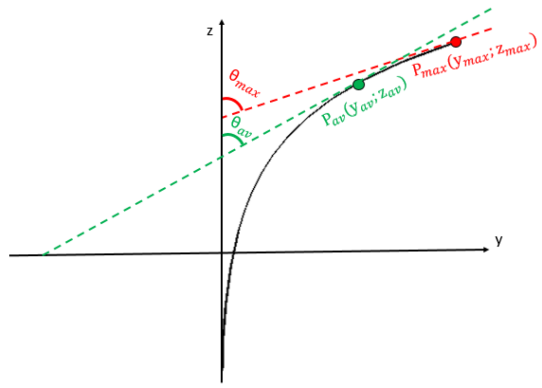

FIGURE 12. End point (red) and average (green) tilt angles and associated tangent lines for Vivaldi 100mm

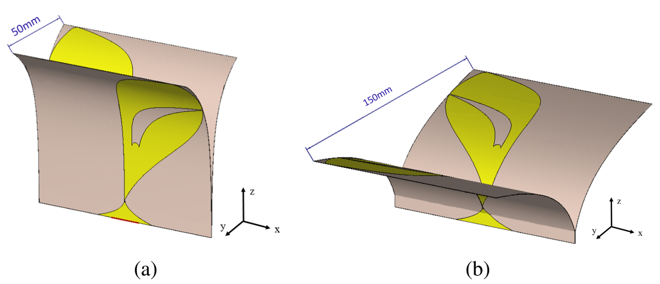

FIGURE 13. H-plane Vivaldi curved array at (a) d=50mm; (b) d=150mm

Fig. 15. At 1GHz both $d = 100mm$ and $d = 150mm$ Vivaldi curved array configurations have a similar value of directivity, but the $d = 50mm$ case has less directivity. This is due to the quasi-omnidirectionnal radiation pattern of the Vivaldi antenna in H-plane, so the tilting phenomenon has nearly no effect which means that the array factor is predominant on the directivity level. Between 1 and 2 GHz, the $d = 150mm$ setup exhibits the highest directivity of the three Vivaldi cases, followed by $d = 100mm$ and finally $d = 50mm$, while the oblique $d = 150mm$ has the most directivity until 1.5 GHz. However, we can see a fall of directivity after 2.5 GHz for the oblique case, which is caused by the tilting phenomenon appearing at 3 GHz.

From 4 GHz, both Vivaldi curved arrays $d = 100mm$ and $d = 150mm$ plus the oblique $d = 150mm$ case have a similar behavior. Focusing on the $d = 150mm$ Vivaldi curved array it can be noted that it always has a lower directivity than the oblique despite having the same distance, which can be explained by three phenomena taking place. First, the Vivaldi curved array has a theoretically smaller array factor effect than the oblique array due to the lower spacing in the high frequency region of the antenna, i.e. around the middle of the exponential travelling slot, as shown in Fig. 8b. Secondly, the act of curving the antenna slightly decreases the directivity of the antenna itself because the E-field components are not perfectly aligned on a similar axis as the oblique case. Last but not least, as shown previously in Table. 2, the tilt is improved in the Vivaldi case compared to the oblique one, resulting to a decrease of the array factor, limiting the directivity. Focusing now on the $d = 100mm$ case, even though the array is smaller than the oblique case by $50mm$, the tilt values of

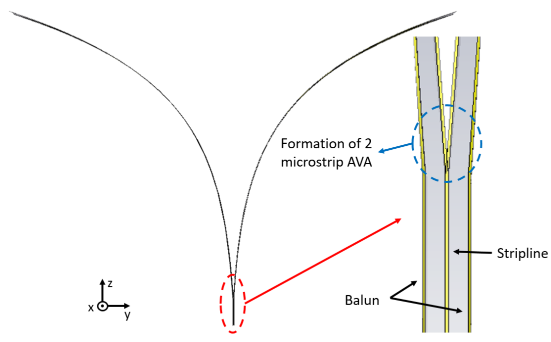

FIGURE 14. Stripline excitation for Vivaldi 100mm

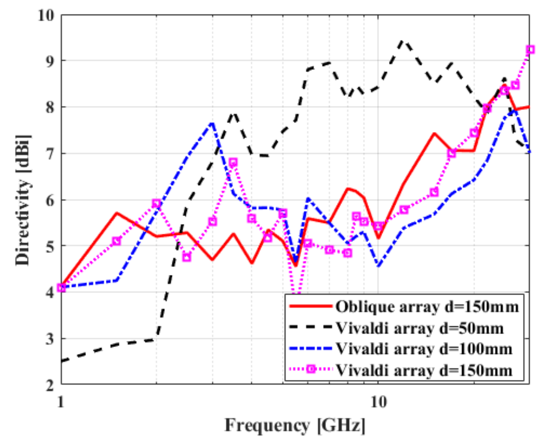

FIGURE 15. Directivity comparison of the Vivaldi curved array at various distances and the oblique array at d=150mm

both arrays are approximately the same ($51.3°$ for the Vivaldi $d = 100mm$ & $52.1°$ for the oblique $d = 150mm$) as shown in Table. 2. However, it still has less directivity than the oblique case due to the first two phenomenons explained above for the $d = 150mm$ Vivaldi curved array, that is a lower spacing in the high frequency region and the curvature of the antenna limiting its inherent directivity. Finally, the $d = 50mm$ Vivaldi curved array achieves the highest directivity between all cases from 3.5 GHz since the tilt is insufficient to significantly decrease the array factor.

To obtain an improved tilting effect in the low frequency region, it is possible to use a 3dB/90° splitter. By creating a 90° phase shift between ports at 1 GHz, the omnidirectional radiation patterns are combined and form a radiation pattern tilted electronically towards ± 90°. As the array factor and tilting effect is dependent on the distance λ_d between antennas, the tilt is well defined in the $d = 150mm$ case at 1 GHz ($d = 0.5\lambda_{1GHz}$), whereas the $d = 50mm$ case presents a tilting effect but with a small array factor ($d = 0.17\lambda_{1GHz}$), Fig. 16a. At frequencies higher than 1 GHz, the electrical tilt is less impactful in the $d = 150mm$ case due to the electrical distance between antennas ($d_{150mm} = 3\lambda_{6GHz}$) and also by the mechanical tilting of the antennas caused by the Vivaldi curvature. However, the distance $d = 50mm$, corresponding to $d = 1\lambda_{6GHz}$, exhibits a $\approx 30°$ tilt at 6 GHz in Fig. 16b, due to the shorter distance d and the fact that the mechanical tilt induced by the Vivaldi curvature is lower.

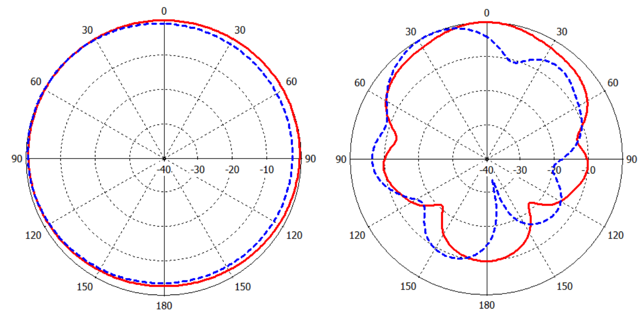

(a)

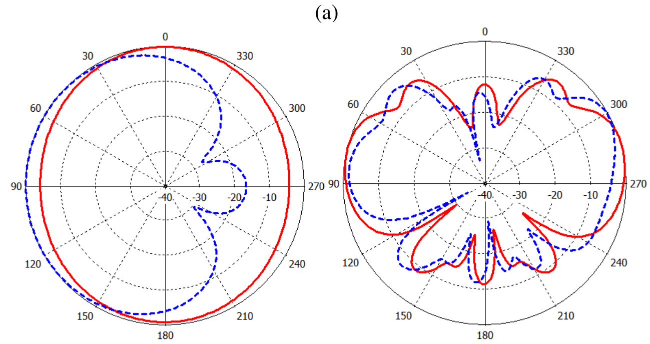

(b)

FIGURE 16. Normalized H-plane radiation pattern of the Vivaldi curved array arrangements with in-phase excitation (red line) and 90° phase shift (blue dots) at respectively 1 GHz and 6 GHz, (a) d=50mm; (b) d=150mm

IV. RESULTS AND DISCUSSION

To assess the effectiveness of the proposed array, two Vivaldi antennas were fabricated and assembled with a stripline excitation, as depicted in Fig. 17a. The PET substrate has been made very thin (0.128mm thickness) to be easily bendable. To achieve the desired Vivaldi curvature, Styren foams were cut into various Vivaldi shapes at different distances ($d = 50mm$; $100mm$ & $150mm$) using a heated wire technique, Fig. 17b. Heated wire technique is one of the most efficient and quick ways to process foam materials with high accuracy, allowing to match the Vivaldi curvature of the simulation's. To maintain this configuration during measurements, the antenna is pressed with the top part of the foam with nylon screws. An illustration of the array bent along the $d = 100mm$ configuration is represented in Fig. 17c.

The measurement of the return loss parameter of the antenna is performed using a PNA N5222B with a frequency range of 10 MHz to 26.5 GHz. A very good agreement between both simulated and measured return loss is shown in Fig. 18. The measured return loss of the antenna, bent along a Vivaldi curvature at a distance of $d = 50mm$ is also presented, showing results very similar to those of the planar antenna. This demonstrates that bending the antenna has minimal impact on its return loss.

The radiation patterns of three Vivaldi curved array arrangements $d = 50mm$, $d = 100mm$ and $d = 150mm$ have been measured over frequency and compared to the simulated radiation patterns in Fig. 19, and show a good agreement between simulation and measure. These measurements were performed using MVG StarLab 600 MHz - 18 GHz through near-field to far-field post-processing, Fig. 20. The different

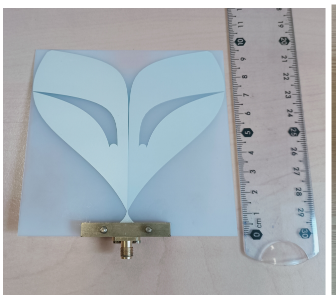

(a)

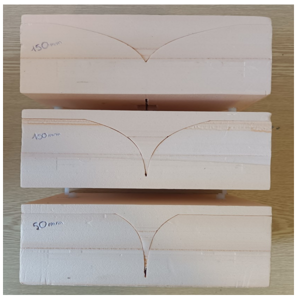

(b)

(c)

FIGURE 17. a) Fabricated Vivaldi array; b) Foams with Vivaldi shapes; c) Array bent along the d=100mm Vivaldi curvature

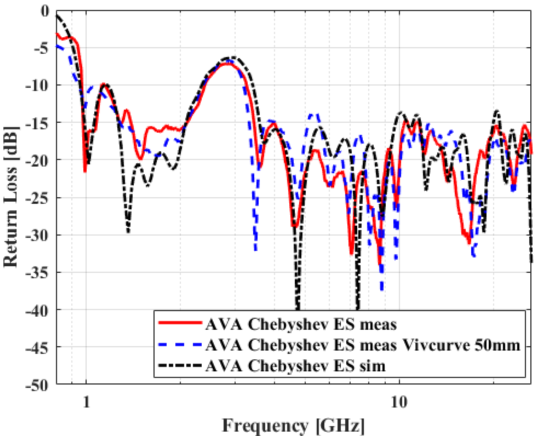

FIGURE 18. Simulated and measured return loss of the AVA Chebyshev ES

effects of the Vivaldi curvature over distance and frequency can be seen, starting with the directivity enhancement at 1.5 GHz as the distance increases, Fig. 19a. At 3 GHz, the Vivaldi curvature creates different types of radiation pattern depending on the distance chosen, as shown in Fig. 19b. The tilting effect starts taking place for the $d = 150mm$ case where we can see a formation of two symmetrical patterns towards both sides, whereas $d = 100mm$ is still directive. At 6 GHz, the radiation pattern of $d = 100mm$ is wider than previous frequencies, due to the tilting effect which is not high enough to induce two symmetrical patterns like the $d = 150mm$ case, Fig. 19c. Focusing on the $d = 50mm$ case, we can see that we managed to obtain a large and quasi-stable radiation pattern for all frequencies. The cross polarisation of the measures is higher than in simulation due to reflections on the RF connector and cable in the anechoid chamber.

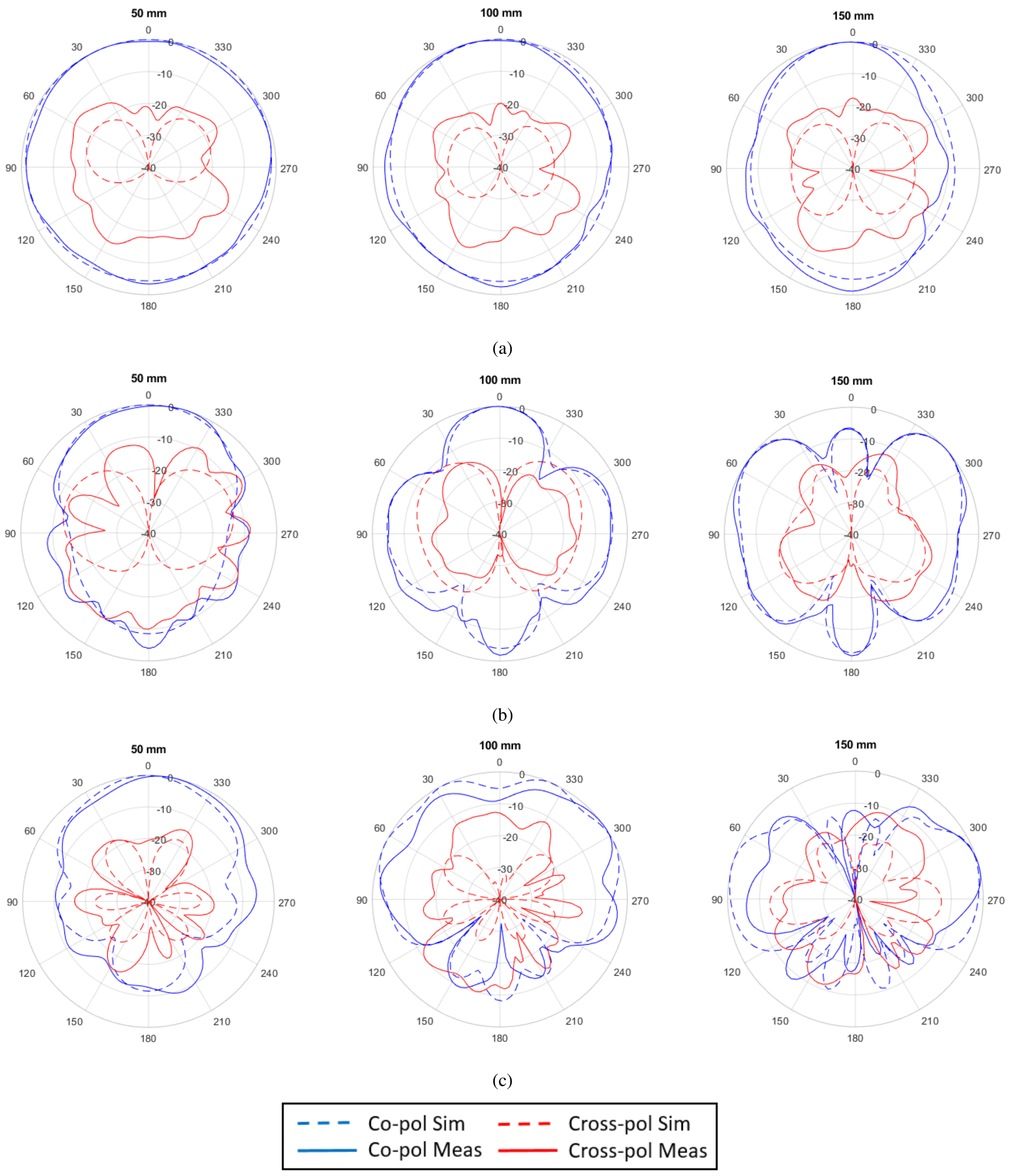

FIGURE 19. Normalized simulated and measured H-plane radiation patterns of the Vivaldi curved array at various distances *d* at (a) 1.5 GHz; (b) 3 GHz; (c) 6 GHz

The directivity of the Vivaldi curved array at various distances is also measured and compared to the simulation, where we can see a good agreement for all cases in Fig. 21.

Finally, a measure in the MVG Starlab with a 3dB/90° splitter working from 0.5 to 7 GHz has been performed on the Vivaldi curved array at distance $d = 150mm$. At 1 GHz, the radiation pattern is electronically tilted by +60°, but does not form the typical cardioid shape as seen in simulation, which is assumed to be due to reflection of EM waves on the splitter in the anechoid chamber, Fig. 22a. At 6 GHz, both radiation patterns are similar due to the high value of mechanical tilt produced by the Vivaldi curvature, Fig. 22b.

V. CONCLUSION

In this study, a Vivaldi antenna with a Chebyshev tapering and exponential slots was proposed for beamforming applications. The Chebyshev profile and the exponential slots allows an enhancement of the impedance in the lowest operating frequency with compact dimensions of 95mm x 100mm. This antenna is curved along a Vivaldi curvature, which creates a mechanical beam tilt. An array arrangement of two antennas along a Vivaldi curvature was created, which allowed to

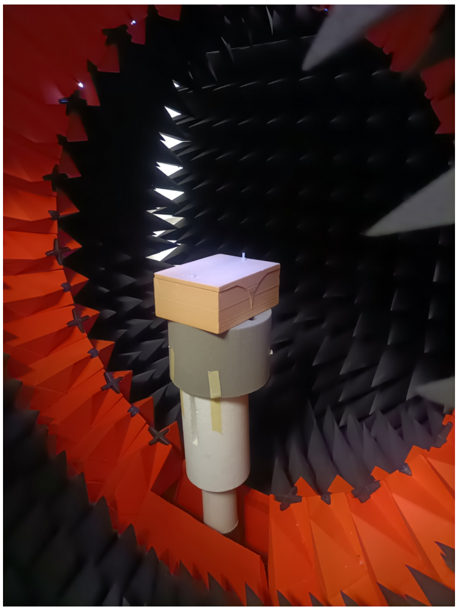

FIGURE 20. Vivaldi curved array at distance d=100mm in the MVG Starlab

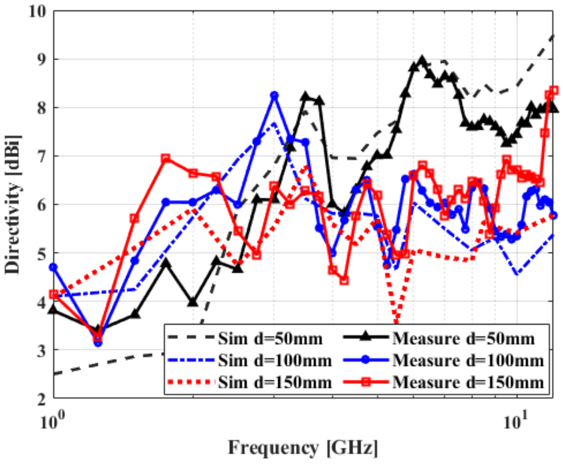

FIGURE 21. Simulated and measured directivity of Vivaldi curved array at various distances

increase the directivity of the Vivaldi curved array at low frequency and to beamform the radiation pattern with different shapes in the upper frequency band, depending on the distances chosen. A comparison is performed and showed that the Vivaldi shape array has a better compactness for the same tilt angle than an oblique arrangement array. A 3dB/90° splitter is also used to significantly tilt the radiation pattern of this array in low frequencies. A good agreement is met between simulated and measured radiation patterns and directivity.

ACKNOWLEDGMENT

The authors would like to thank the company Seribase for the manufacturing of the antennas on PET substrate and the company BORRAX for the wire cutting on Styren foams.

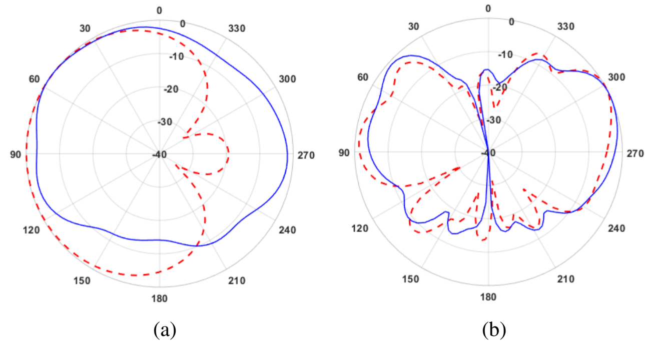

FIGURE 22. Normalized H-plane simulated (red dots) and measured (blue line) radiation patterns with 3dB/90° splitter of the Vivaldi $d = 150mm$ array at a) 1 GHz; b) 6 GHz

REFERENCES

[1] S. Kirthiga and M. Jayakumar, “Performance of Dualbeam MIMO for Millimeter Wave Indoor Communication Systems,” *Wireless Pers Commun.*, vol. 77, no. 1, pp. 289–307, Jul. 2014, DOI = 10.1007/s11277-013-1506-0.

[2] Z. Wani and M. P. Abegaonkar and S. K. Koul, “Dual-Beam Antenna for Millimeter Wave MIMO Applications,” *2018 IEEE Indian Conference on Antennas and Propogation (InCAP).*, pp. 1–3, Dec. 2018. DOI = 10.1109/INCAP.2018.8770883.

[3] W. Hong et al., “Multibeam Antenna Technologies for 5G Wireless Communications,” *IEEE Trans. Antennas Propagat.*, vol. 65, no. 12, pp. 6231–6249, Dec. 2017, DOI = 10.1109/TAP.2017.2712819.

[4] P. J. Gibson, "The Vivaldi Aerial," *1979 9th European Microwave Conference, Brighton.*, pp. 101-105, 1979. DOI = "10.1109/EUMA.1979.332681".

[5] E. Gazit, "Improved design of the Vivaldi antenna," *IEE PROCEEDINGS.*, vol. 135, no. 2, pp. 89, 1988. DOI = "10.1049/ip-h-2.1988.0020".

[6] A. Gorai and A. Karmakar and M. Pal and R. Ghatak, "A super wideband Chebyshev tapered antipodal Vivaldi antenna," *AEU - International Journal of Electronics and Communications.*, vol. 69, no. 9, pp. 1328-1333, 2015. DOI = "10.1016/j.aeue.2015.05.017".

[7] D. H. Schaubert and W. Elsallal and S. Kasturi and A. O. Boryssenko and M. N. Vouvakis and G. Paraschos, "Wide bandwidth arrays of Vivaldi antennas," *IET Seminar on Wideband, Multiband Antennas and Arrays for Defence or Civil Applications.*, pp. 1-20, 2008. DOI = "10.1049/ic:20080084".

[8] D. Yang and S. Liu and D. Geng, “A Miniaturized Ultra-Wideband Vivaldi Antenna With Low Cross Polarization,” *IEEE Access.*, vol. 5, pp. 23352–23357, 2017, DOI = 10.1109/ACCESS.2017.2766184.

[9] Sang-Gyu Kim and Kai Chang, "A low cross-polarized antipodal Vivaldi antenna array for wideband operation," *IEEE Antennas and Propagation Society Symposium.*, vol. 3, pp. 2269-2272, 2004. DOI = "10.1109/APS.2004.1331823".

[10] Sun Hai-Han and Yee Hui Lee and Wenhao Luo and Lai Fern Ow and Mohamed Lokman Mohd Yusof and Abdulkadir C. Yucel, "Compact Dual-Polarized Vivaldi Antenna with High Gain and High Polarization Purity for GPR Applications," *Sensors.*, vol. 21, no. 2, pp. 503, 2021. DOI = "10.3390/s21020503".

[11] J. D. S. Langley and P. S. Hall and P. Newham, "Balanced antipodal Vivaldi antenna for wide bandwidth phased arrays," *IEE Proc., Microw. Antennas Propag.*, vol. 143, no. 2, pp. 97, 1996. DOI = "10.1049/ip-map:19960260".

JULIEN HAREL was born in Brest, France, in 1998. He graduated in electrical engineering and radio communications from the Ecole Supérieur d'ingénieur de Rennes (ESIR) and received the Master's degree in telecommunication and electronics in 2021. Since 2021, he has been working toward the Ph.D. degree at the Institut d'Electronique et des Technologies du numéRique (IETR), University of Rennes, Rennes, France. His current research fields are UWB compact antennas and direction findings applications.

MOHAMED HIMDI received the Ph.D. degree in signal processing and telecommunications from the University of Rennes 1, France in 1990. Since 2003, he has been a Professor with the University of Rennes 1, and the Head of the High Frequency and Antenna Department until 2013, and from 2024 of IETR. He has authored or co-authored 170 journal papers and over 350 papers in conference proceedings. H-index 38. He has also co-authored 12 book chapters. He holds 49 patents. His research activities concern passive and active millimeter-wave antennas. His research also includes the development of new architectures of antenna arrays, and new three-dimensional (3-D) antenna technologies. He was Laureate of the 2d National Competition for the Creation of Enterprises in Innovative Technologies in 2000 (Ministry of Industry and Education). In March 2015 he received the JEC-AWARD at Paris on Pure composite material antenna embedded into a motorhome roof for the Digital Terrestrial Television reception. He received the Innovation Trophy 2021 from University of Rennes 1.

OLIVIER LAFOND received the Ph.D. degree in Signal Processing and Telecommunications from the University of Rennes 1, Rennes, France, in 2000. Since October 2002, he has been an associate professor at the IETR, University of Rennes. Since 2020, he has been a full professor at IETR. He has authored or co-authored 47 journal papers and 67 papers in conference proceedings. He has also authored/co-authored four book chapters and holds eight patents in the area of antennas. His research activities concern passive and active millimeter-and submillimeter-wave antennas, quasi-optical systems (inhomogeneous lens), and plasma antennas. Prof. Lafond has been responsible for one ESOA course since 10 years concerning millimeter-wave antennas.

OLIVIER CLAUZIER received the Ph.D. degree in Signal Processing and Telecommunications from the University of Rennes 1, France in 2012. Since 2018, he has been a radiofrequency engineer at AVANTIX.

OLIVIER VIVARES received the master degree in Propagation, Telecommunication, Teledetection from the University of Sophia Antipolis in 1996. Since 2018 he has been the head of the radiofrequency expertise division at AVANTIX.

• • •